

Evaluation of chemical-kinetics models for *n*-heptane combustion using a multidimensional CFD code

Viswanath R. Katta^{a,*}, Suresh K. Aggarwal^b, William M. Roquemore^c

^a Innovative Scientific Solutions, Inc., Dayton, OH 45440, United States

^b Department of Mechanical Engineering, University of Illinois at Chicago, Chicago, IL, United States

^c Propulsion Directorate, Wright-Patterson Air Force Base, OH 45433, United States

ARTICLE INFO

Article history:

Received 27 September 2010

Received in revised form 24 September 2011

Accepted 20 October 2011

Available online 7 November 2011

Keywords:

Heptane combustion

Chemical kinetics

Modeling

Diffusion flames

Premixed flames

ABSTRACT

Computational fluid dynamics (CFDs)-based predictions are presented for nonpremixed and partially premixed flames burning vaporized *n*-heptane fuel. Three state-of-the-art chemical kinetics models are incorporated into a time-dependent, two-dimensional, CFD model known as UNICORN. The first mechanism is the San Diego (SD) mechanism (52 species and 544 reactions), the second one is the Lawrence Livermore National Laboratory (LLNL) mechanism (160 species and 1540 reactions), and the third one is the National Institute of Standards and Technology (NIST) mechanism (197 species and 2926 reactions). Soot model based on acetylene, and radiation model based on optically thin media assumption are included. Two-dimensional calculations are made for the detailed structures of nonpremixed and partially premixed flames, strain-induced extinction and diffusion-controlled autoignition and the results are compared with the available experimental data. Diffusion-controlled autoignition characteristics are also compared with the ignition delay times calculated in homogeneous stoichiometric mixture of *n*-heptane and air. Through the simulation of complete flowfields between the opposing fuel and air ducts reasons for the flame curvature seen in some experiments are explained. Compared to the traditional one-dimensional models for opposing-jet flames, two-dimensional simulations are found to give results closer to the experimental values when the flames are highly stretched. While LLNL mechanism predicted extinction of a nonpremixed flame better, NIST mechanism predicted the autoignition behavior in the flowfield established by the opposing jets of fuel and heated air better. However, all three mechanisms predicted both the nonpremixed and partially premixed *n*-heptane flames very well. Surprisingly, SD mechanism with less than one-third of the species used in the other two mechanisms predicted flame structures with nearly the same accuracy. Comparisons made with the available experimental data could not suggest which mechanism is better in predicting the minor species concentrations. Computations could not predict the temperature rise detected in the experiments in the premixed-combustion zone of a partially premixed flame when it was subjected to a moderately high stretch rate.

© 2011 Elsevier Ltd. All rights reserved.

1. Introduction

Detailed chemical kinetics for describing combustion of hydrocarbon fuels involves several hundred species and several thousand elementary reactions. Accurate chemical-kinetics models help not only in understanding the combustion phenomena but also for modeling the combustion processes in various practical devices and, thereby, making combustion more efficient and less polluting. The need for more accurate and presumably larger chemical-kinetic mechanisms is being strongly driven by the escalating costs of petroleum-based fuels and the search for alternate and renewable fuels. Significant progress has been reported in recent years in the development of detailed reaction mechanisms

for simple as well as complex hydrocarbon fuels. A considerable part of this effort has focused on the oxidation chemistry of methane (CH₄) and *n*-heptane (*n*-C₇H₁₆), as these two fuels are considered as the most representative gaseous and liquid fuels, respectively. Moreover, methane is the dominant constituent of natural gas, while *n*-heptane is a primary reference fuel for octane rating in internal combustion engines, and also a good surrogate for gasoline [1,2] and diesel [3,4] fuels. Consequently, several detailed mechanisms have been developed and validated for these two fuels. The mechanisms for methane oxidation include GRI-3.0 [5], HPNGB-1 [6], and Curran [7] mechanisms. Similarly, several detailed reaction mechanisms have been reported for *n*-heptane oxidation [8–10].

Detailed chemical-kinetics mechanisms for fuels are generally validated using some specific targets, such as flow reactor data, ignition delay times from shock tube experiments, and laminar

* Corresponding author. Tel.: +1 9372558781.

E-mail address: vrkatta@gmail.com (V.R. Katta).

flame speeds. The validation process then involves performing zero- and one-dimensional simulations using codes such as RUN1DL [11], OPPDIF [12], and CHEMKIN [13] and comparing the results with the available experimental data. Extensive experimental data for the intermediate species concentrations are required for obtaining a reasonably built or validated kinetics mechanism. However, it is not always feasible to obtain concentrations of the numerous hydrocarbon intermediates generated during the combustion of complex hydrocarbon fuels. As a result, validation of complex chemical-kinetics mechanisms using the traditional zero- and one-dimensional experimental/numerical studies can be performed only partially. Alternatively, one could include more target flames, such as coaxial nonpremixed [14], Bunsen [15], and center-body flames [16], and validate the mechanisms for predicting flame shapes, lift-off heights, blowout characteristics, temperature and species distributions, etc. Most of these data can be obtained using measurement techniques ranging from inexpensive (direct photographs) to expensive (laser diagnostics) techniques.

The main reason why researchers are restricting themselves to zero- and one-dimensional data for validating a given chemical-kinetics mechanism stems from modeling limitations. The additional target flames listed above are all of multidimensional in nature and can only be simulated using two- or three-dimensional codes. In fact, calculation of multidimensional flames using detailed chemistries is known since 1960s [17] and the need for understanding combustion phenomena such as flame stability, pollutant formation, and re-ignition have led to the development of CFD codes with detailed chemical kinetics [18–21]. However, due to the fact that computational time increases significantly with the size of the chemical-kinetics mechanism used, CFD code developments are limited to either simple fuels such as hydrogen [22], methane [23], and ethylene [24] that are described with smaller detailed mechanisms (less than 100 species) or to complex fuels such as propane [25], heptane [26], and JP-8 [27] that are described with reduced mechanisms (tens of species). On the other hand, computer hardware technology has advanced significantly during the past decade and desktop cpu with hundreds of cores [28] could become available in the next 10 years or so-paving roads for computing multidimensional flames using hundreds of species and thousands of reactions routinely. Recently, Katta and Roquemore [29] have demonstrated feasibility of such simulations through adopting efficient algorithms for faster and error-free calculations with large chemical-kinetics mechanisms. The present paper is aimed at (1) demonstrating the current ability to perform detailed chemical-kinetics validation studies using a multidimensional code and (2) to understand the accuracies of the existing mechanisms for *n*-heptane fuel in simulating various types of combustion phenomenon.

There is a considerable interest in understanding *n*-heptane combustion as it is treated as a primary reference fuel for octane rating in internal combustion engines. Numerous investigators have developed chemical-kinetic mechanisms describing the oxidation of *n*-heptane [8–10]. Extensive experimental work has also been performed for validating/developing these detailed mechanisms [30–32]. In the present paper three mechanisms developed by University of California at San Diego, Lawrence Livermore National Laboratory, and National Institute of Standards and Technology are incorporated into a two-dimensional CFD code, UNICORN (UNsteady Ignition and COmbustion using ReactioNs), and investigated their ability to predict chemical and thermal structures of nonpremixed and partially premixed flames, extinction limits, and ignition characteristics.

2. Mathematical model

UNICORN code [29,33,34] is a time-dependent, axisymmetric mathematical model, which is used for the simulation of unsteady

reacting flows. It is capable of performing direct numerical simulations (DNSs) and has been developed/improved over several years. Its evolution has been in conjunction with experiments conducted to test its ability to predict ignition, extinction, stability limits, and the dynamic characteristics of nonpremixed and premixed flames of various fuels. It solves for *u*- and *v*-momentum equations, continuity, and enthalpy- and species-conservation equations on a staggered-grid system. The body-force term due to the gravitational field is included in the axial-momentum equation for simulating vertically mounted flames. A clustered mesh system is employed to trace the large gradients in flow variables near the flame surface. Details of the finite-differencing schemes and the methodologies used for handling stiff species-conservation equations are given in Refs. [29] and [34].

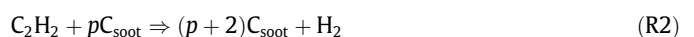
Three detailed chemical-kinetics models developed for heptane combustion are incorporated into UNICORN. First one is San Diego (SD) mechanism [35]. It consists of 52 species and 544 elementary reactions. The second one is Lawrence Livermore National Laboratory (LLNL) mechanism [36]. It consists of 160 species and 1540 reactions. And the third one is National Institute of Standards and Technology (NIST) mechanism [37]. It consists of 197 species and 2926 reactions. These three mechanisms were chosen as they represent state-of-the-art semi-detailed and detailed chemistries for *n*-heptane combustion. The thermodynamic properties such as enthalpy and specific heats of all the species are calculated from the polynomial curve fits developed for the temperature range 300–5000 K. The transport properties such as viscosity, thermal conductivity and binary molecular diffusion coefficients for each species are evaluated using Chapman–Enskog treatment for colliding molecules and Lennard–Jones potentials and reduced temperatures as described in Ref. [38]. Mixture viscosity and thermal conductivity are then estimated using the Wilke and Kee expressions, respectively. Molecular diffusion is assumed to be of the binary-diffusion type, and the diffusion velocity of a species is calculated using Fick's law and the effective-diffusion coefficient of that species in the mixture.

Soot formation is described using two transport equations, one for the particle number density, N_s , and the second one for the soot mass fraction, Y_s . These equations can be written for unsteady flow as

$$\frac{\partial \rho N_s}{\partial t} + \nabla \cdot (\rho V N_s) - \nabla \cdot (\rho D_s \nabla N_s) = \omega_{N_s} \quad (1)$$

$$\frac{\partial \rho Y_s}{\partial t} + \nabla \cdot (\rho V Y_s) - \nabla \cdot (\rho D_s \nabla Y_s) = \omega_s \quad (2)$$

where V is the velocity vector, ρ is density, D is the molecular diffusion coefficient, and ω is the production term from chemical reactions. The two source terms in Eqs. (1) and (2) are obtained using the following inception-growth-oxidation approach of Lindstedt [39],



In the above mechanism R1 describes nucleation process, R2 growth process, R3–R5 oxidation process, and R6 agglomeration

process. Here, C_{soot} represents gaseous soot particles, and the coefficients p and q are used for describing the particle growth and agglomeration processes, respectively. A simple radiation model [40] for gaseous species (including soot), based on the optically thin-media assumption [41], is incorporated into the energy equation. Only radiation from CH_4 , CO , CO_2 , H_2O , and soot is considered in the present study. The radiation source term (q_r) is then calculated as

$$q_r = -Cf_v T^5 - \sum k_{p_i} \sigma T^4, \quad (3)$$

where f_v is soot volume fraction, C is a constant calculated based on spectral absorption coefficient of soot [42,43], σ the Stefan–Boltzmann constant, and k_{p_i} the Planck mean absorption coefficient of the i th species [40]. Detailed radiation studies on ethylene jet diffusion flames conducted by Liu et al. [44] suggested that the radiation model used in the present study (optically thin model) could result in less than 2% error in soot volume fraction and 50 K in peak temperature when compared to more sophisticated discrete-ordinates radiation models [44].

The finite-difference forms of the momentum equations are obtained using an implicit QUICKEST scheme [34,45], and those of the species and energy equations are obtained using a hybrid scheme of upwind and central differencing. At every time step, the pressure field is accurately calculated by solving all the pressure Poisson equations simultaneously and using the LU (Lower and Upper diagonal) matrix-decomposition technique. Different types of boundary conditions such as adiabatic wall, isothermal wall, symmetric surface, outflow, and inflow can be applied to the boundaries of the computational domain [46].

3. Results and discussion

Multidimensional-flame simulations using UNICORN are performed on a Personal Computer with an AMD Opteron-250 cpu and 2.0 GB of memory. Execution times strongly depend on the number of species considered in the chemical-kinetics model and the grid size. Typical execution times using a mesh of 15 K nodes and with the SD, LLNL, and NIST mechanisms are 8, 23, and 30 s/time-step, respectively. Steady state solutions are typically obtained in about 4000 time steps starting from the solution obtained using the global combustion chemistry model. Calculations made with different heptane chemical kinetics models are presented in the following subsections.

3.1. Nonpremixed flame structure

The nonpremixed flame considered for validating the numerical models is a flat flame formed between the opposing jets of pre-vaporized n -heptane and air. Seiser et al. [30] have conducted experiments on this laminar flame and obtained temperature and species measurements along the axis of symmetry (centerline). They performed one-dimensional calculations for the flame structures along the centerline using a shortened version of SD mechanism [30]. In their further studies [31] of these flames they also used LLNL mechanism and a larger version of it having 282 species [36]. The burner was made up of two opposing ducts with inner diameters of 22.2 mm through which reactants were introduced separately. The distance between the ducts at the exits was 10 mm. A known mixture of n -heptane vapor and nitrogen was introduced from the bottom duct while air was introduced from the top duct. The temperatures of the fuel and air jets were 338 and 298 K, respectively. Experiments were conducted for different global strain rates (k) through varying the jet velocities while satisfying the following conditions

$$\text{StrainRate } k = \frac{2|V_2|}{L} \left(1 + \frac{|V_1|}{|V_2|} \sqrt{\frac{\rho_1}{\rho_2}} \right) \quad (4)$$

$$\text{and } \sqrt{\rho_1}|V_1| = \sqrt{\rho_2}|V_2| \quad (5)$$

While Eq. (4) defines global strain rate, Eq. (5) enforces momentums of the fuel and oxidizer jets to be equal for keeping the flame at the midsection of the burner. Here, V_1 and V_2 represent the velocities of the fuel and air jets, respectively and ρ_1 and ρ_2 represent the densities of the respective jets. L is the separation distance between the fuel and oxidizer ducts.

A two-dimensional modeling of the opposing-jet flame requires jet exit velocities. Since the experimental data reported in [30] and [31] for these flames are in terms of strain rate, the jet exit velocities are calculated using Eqs. (4) and (5) while densities of the fuel and oxidizer jets are calculated from the measured temperatures and ideal gas law at standard pressure. For model validation purpose the flame established at a moderate strain rate of 150 s^{-1} is considered. Fuel used for this flame contained 15% heptane and 85% nitrogen. The fuel and air velocities, as determined from Eqs. (4) and (5), are 0.342 and 0.375 m/s, respectively. Velocity for the N_2 curtain flow surrounding the fuel and oxidizer jets was set as 0.1 m/s. Simulations for the flowfield between the upper and lower ducts are performed using a 301×41 variable grid system, which yielded a uniform spacing of $33 \mu\text{m}$ in the axial direction and expanding spacing with a minimum of $100 \mu\text{m}$ in the radial direction. Calculations are performed using the SD, LLNL, and NIST chemical kinetics models. The three steady state flames obtained are shown in Fig. 1. Temperature distributions between 300 and 1800 K are plotted using rainbow color scheme. A comparison among the temperature distributions shown in Fig. 1 reveals that the three mechanisms have resulted in flames that are nearly identical in shapes and sizes. The nonpremixed flame formed between the opposing reactant ducts is nearly flat (planar); however, a close observation indicates that it is slightly curved upward toward air duct. As described in the previous section, gravitational force in the axial direction is included in the calculations and the observed flame curvature, at first sight, might appear to be developing because of buoyancy. However, calculations repeated after turning off the gravitational forces also resulted in a curved flame identical to that shown in Fig. 1, which, suggested that the curvature to the flame surface did not develop because of buoyancy.

Based on stoichiometry it is known that about 11 mol of oxygen are needed for burning one mole of heptane. Because of such high

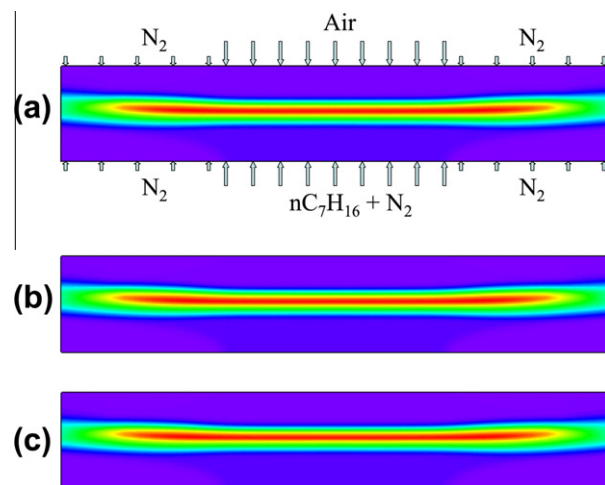


Fig. 1. Opposing-jet nonpremixed heptane flame simulated using (a) SD, (b) LLNL, and (c) NIST mechanisms. Global strain rate is 150 s^{-1} . Temperature distributions are shown between 300 and 1800 K.

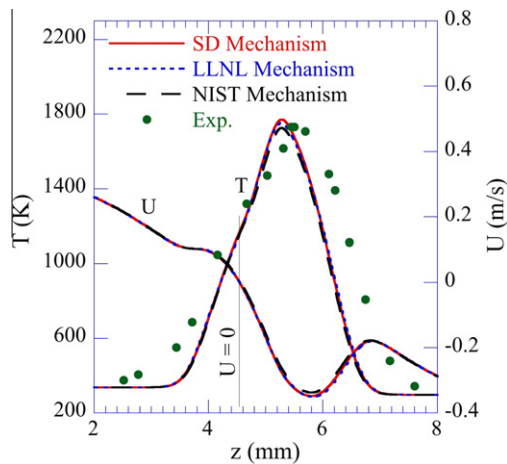


Fig. 2. Distributions of temperature and axial velocity plotted along the centerline. Lines represent flames computed using different chemical kinetics mechanisms and symbols represent measurements of Seiser et al. [30]. Global strain rate is 150 s^{-1} .

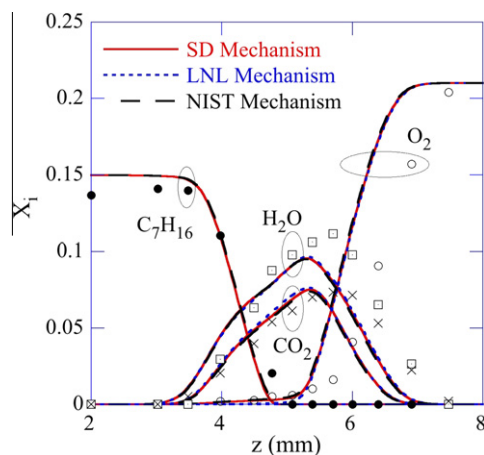


Fig. 3. Distributions of fuel, oxygen, H_2O , and CO_2 plotted along the centerline. Lines represent flames computed using different chemical kinetics mechanisms and symbols represent measurements of Seiser et al. [30]. Global strain rate is 150 s^{-1} .

requirement for oxygen nonpremixed flame in the opposing-jet burner establishes on the airside of the stagnation plane (surface along which the axial velocity component is zero). Consequently, the volumetric expansion occurring along the flame surface will be more on the airside of the stagnation plane. The additional momentum generated by the hot gases toward the stagnation plane moves the stagnation point (where axial as well as radial component of velocity are zero) closer to the fuel jet and makes the stagnation plane (and also the flame surface) curve toward the air jet. Shift in the location of the stagnation point from the mid section of the burner is evident in Fig. 2.

Temperature and axial-velocity distributions along the centerline across the flame are shown in Fig. 2. While the computed profiles are shown using lines, temperature measurements obtained by Seiser et al. [30] are plotted with solid symbols. Even though the moments of the fuel and air jets were matched, the stagnation point ($U=0$) is located $\sim 0.5 \text{ mm}$ away from the midsection ($z=5 \text{ mm}$) toward the fuel duct. The peak-temperature surface is located $\sim 0.2 \text{ mm}$ away from the midsection toward the air duct, which is also the case in the experiment. All three mechanisms resulted in nearly identical temperature and velocity profiles, which is as expected since the main heat-release steps in these mechanisms are validated for heptane-air combustion. On the other hand, formation mechanisms of minor species in the three

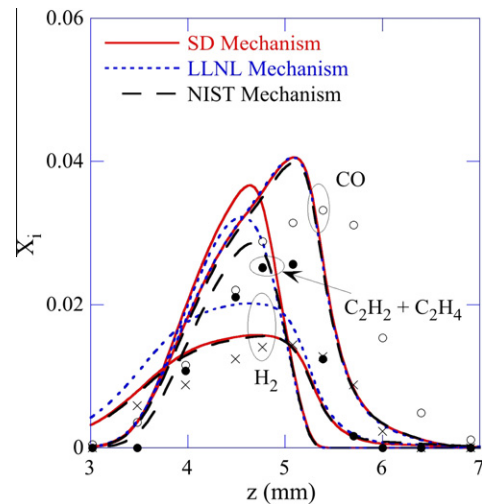


Fig. 4. Distributions of intermediate fuel species H_2 , $\text{C}_2\text{H}_2 + \text{C}_2\text{H}_4$, and CO plotted along the centerline. Lines represent flames computed using different chemical kinetics mechanisms and symbols represent measurements of Seiser et al. [30]. Global strain rate is 150 s^{-1} .

kinetics models are less validated and one might expect some variations in their predictions. Calculated peak temperature values compare well with the measurements. However, flame in the experiment seems to be broader and shifted by $\sim 0.2 \text{ mm}$ toward the air duct. Interestingly, the one-dimensional calculations performed by Seiser et al. [30] also resulted in a temperature profile similar to the predictions shown in Fig. 2—suggesting that one-dimensional assumption for this nearly flat, moderately stretched flame is reasonable. Maximum temperature predicted by the NIST mechanism is $\sim 40 \text{ K}$ lower than those obtained with the SD and LLNL mechanisms (Fig. 2). This lower temperature caused less volumetric expansion for the combustion products and less increase to velocity (negative) at $z \sim 5.8 \text{ mm}$.

Predicted distributions of fuel, oxygen, H_2O , and CO_2 along the centerline are shown in Fig. 3 along with the measured ones. Once again, all three chemical-kinetics models predicted nearly the same distributions for these species. Comparisons with experiment are also reasonable, even though, H_2O concentration was under-predicted. Similar to the differences noted in temperature data (Fig. 2), measured species profiles are broader and shifted toward the air duct. It is important to note that measurements for temperature and species concentrations were made using different probes—suggesting that observed differences between the measurements and computations are beyond the experimental errors. However, since both the probes used for the measurements (thermocouple and quartz microprobe [30]) are intrusive type, the uncertainty with regard to the perturbation to the flame in the experiment remains. It is also possible that the H_2 -species chemistry/transport is not adequately represented in these mechanisms. Diffusion of H_2 further into the air jet than what the models are predicting could also result in shifts in the peaks of water concentration and temperature closer to the air inlet. Nevertheless, as described in the Mathematical-Model section, the transport properties of the individual species in these simulations were estimated using rather sophisticated molecular theory and corrections to their values needs investigations at fundamental level. Overall, it may be considered that all three chemical-kinetics mechanisms are resulting in the same distributions for the major species shown in Fig. 3 even though there are some differences in the temperature predictions (Fig. 2).

Comparisons between the predictions and measurements for some other species such as fuel fragments and radicals are shown

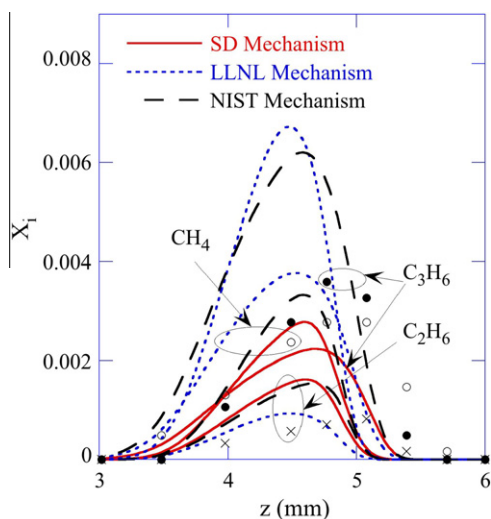


Fig. 5. Distributions of intermediate species CH_4 , C_3H_6 , and C_2H_6 plotted along the centerline. Lines represent flames computed using different chemical kinetics mechanisms and symbols represent measurements of Seiser et al. [30]. Global strain rate is 150 s^{-1} .

in Fig. 4 and 5. Distributions of H_2 , CO and $\text{C}_2\text{H}_2 + \text{C}_2\text{H}_4$ are plotted in Fig. 4 and those of CH_4 , C_3H_6 and C_2H_6 are shown in Fig. 5. In general, models are over predicting the concentrations for these species. Note, similar discrepancies between measurements and calculations were also reported by Seiser et al. [30] in their one-dimensional simulations using CHEMKIN and a shortened version of SD mechanism [47]. Consistent with the differences noted between the experiment and simulations for the temperature and major species concentrations, measured distributions for H_2 and CO are also shifted closer to the air inlet. While SD and NIST mechanisms in the present two-dimensional simulations predicted concentrations for H_2 close to those measured, LLNL mechanism predicted nearly 25% higher concentration. On the other hand, NIST mechanism's prediction for total concentration of C_2H_2 and C_2H_4 is lower when compared to the other two mechanisms, but closer when compared with the measurements. Differences in the predictions made by the three mechanisms become more noticeable for the minor species shown in Fig. 5. Over all, the moderately stretched nonpremixed flame was predicted reasonably well with all the three chemical-kinetics mechanisms and no mechanism is found distinctly more accurate than the others.

3.2. Strain-induced extinction

Using the opposing-jet burner described in the previous section, Seiser et al. [31] obtained limiting strain rates for extinguishing the nonpremixed flames. Selecting a particular value for the *n*-heptane-nitrogen ratio in the fuel jet and fixing the stoichiometric mixture fraction ξ_{st} (defined as $[1 + \frac{11Y_F W_{O_2}}{Y_{O_2} W_F}]^{-1}$, where W_F and W_{O_2} represent the molecular weights of fuel and oxygen, respectively, and Y_F and Y_{O_2} represent the mass fractions fuel and oxygen, respectively) at 0.1, Seiser et al. [31] obtained the ratio between air and nitrogen required in the oxidizer jet. They performed the extinction experiments through varying the fuel and oxidizer jet velocities while allowing only a small change in the flame location by matching the momentums of these jets (Eq. (1)). Calculations for these experiments are performed using UNICORN code for assessing the abilities of the SD, LLNL, and NIST mechanisms in predicting the critical extinction strain rates.

Results obtained for the flame with the highest concentrations of fuel and oxygen used in the experiment are shown in Fig. 6.

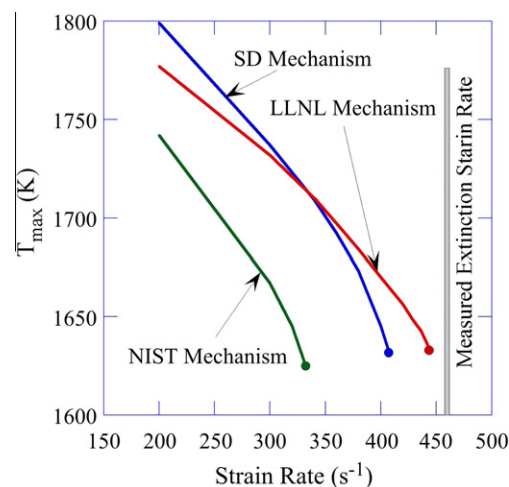


Fig. 6. Maximum flame temperatures obtained at different strain rates. Solid circles represent extinction conditions.

Temperatures of the fuel and oxidizer streams were set as 345 and 298 K, respectively. While the fuel jet was composed of 28.2% *n*-heptane and 71.8% nitrogen by volume, oxidizer jet was composed of 20.5% oxygen and 79.5% nitrogen. A separation distance of 10 mm was maintained between the fuel and oxidizer jets. Calculations for a weakly stretched nonpremixed flame were performed initially after specifying low values for the jet velocities. Stretched flames were then obtained by increasing the fuel and oxidizer jet velocities in steps. Calculations were continued until the flame was extinguished; however, the incremental increases imposed to the velocities were reduced as the flame approached extinction conditions. Extinction strain rates for the three mechanisms were obtained through repeating the calculations starting from the weakly stretched flame.

Due to an imbalance between the heat produced in the flame and heat transported away from the flame, opposing-jet flame gets thinner and its maximum temperature decreases as the strain rate (or velocity) is increased. Changes to the flame temperature with strain rate obtained with three chemical-kinetics mechanisms are shown in Fig. 6. Strain rate and temperature obtained for the critical flame (just prior to extinction) are shown with filled circles. Measured extinction strain rate is shown with a hatched rectangle. Significant differences may be found in the flame responses to stretch obtained with the three mechanisms. LLNL mechanism gave the most stable flame with a critical extinction strain rate of 447 s^{-1} . This value compares well with the measured value of 460 s^{-1} . NIST mechanism, which predicted lowest maximum temperatures in a weakly stretched flame (Figs. 2 and 6), predicted flame extinction at a strain rate of 340 s^{-1} . SD mechanism, which predicted highest temperatures in a weakly strained flame (Figs. 2 and 6), predicted flame extinction at a strain rate of 405 s^{-1} . Interestingly, one-dimensional calculations performed by Seiser et al. [31] for this flame using two versions of LLNL mechanism (159-species version that is identical to the one used in this study and a 282-species version) yielded extinction strain rates close to 520 s^{-1} , which are $\sim 13\%$ higher than the measured value. The two-dimensional simulations performed in this study using the same mechanism resulted in extinction strain rate that is just 3% lower than the measurements. As expected, calculations performed for the diluted flames resulted in flame extinction at lower strain rates and the critical values matched well with the measurements. Note that the one-dimensional calculations performed by Seiser et al. [31] also yielded a better agreement between the measurements and simulations for the extinction strain rates for the

diluted flames. The better agreement between the measurements and calculations made with the two-dimensional model for the larger-extinction-strain-rate cases suggests that the errors associated with the one-dimensional assumption for the opposing-jet flame are becoming significant at higher strain rates. Such differences in measured and predicted (one- and two-dimensional) extinction conditions were also noted in the previous studies of opposing-jet partially premixed flames [48].

Among the three mechanisms considered here, NIST mechanism has the most number of species (197). Yet, it gave the strain rate for extinction much lower than that measured in the experiments. It is important to realize that majority of the species used in large mechanisms appear in flames only in trace amounts. They don't affect the basic combustion processes such as ignition and heat release. However, they are included for making the mechanism useful in predicting other combustion processes such as pollutant formation. The main reason for NIST mechanism to predict flame extinction at stretch rates well below the measured values is evident from Figs. 2 and 6. In general, NIST mechanism under predicts flame temperature by about 50 K. Since flame chemistry is strongly related to temperature, NIST mechanism generates flames that are weaker than those generated by the other two mechanisms and, consequently, they extinguish relatively sooner on a stretch-rate scale. LLNL mechanism, on the other hand, predicted temperatures lower than those of the SD mechanism initially and gradually higher as the stretch rate is increased – leading to the highest extinction stretch rate. Interestingly, all three mechanisms extinguished the flame in Fig. 6 when the peak temperature dropped to 1620 ± 4 K.

3.3. Autoignition

Using the previously described opposing-jet flame configuration Seiser et al. [31] performed experiments for the autoignition of heptane fuel. They issued *n*-heptane-nitrogen mixture from the bottom duct and heated air from the top duct. Autoignition condition was reached by gradually increasing the air temperature. The volume fraction of *n*-heptane in the fuel jet was kept constant at 15% while the fuel temperature was maintained at 378 K. Experiments were performed for different strain rates. For validation purpose calculations for this configuration are performed for a strain rate of 400 s^{-1} . This strain rate corresponds to a fuel jet velocity of 0.57 m/s and to a 1264-K air jet velocity of 1.2 m/s. Two-dimensional simulations for autoignition using SD, LLNL, and NIST mechanisms are performed by gradually increasing the air temperature. Since autoignition depends not only on temperature but also on induction time, calculations for this problem must be performed sufficiently long – well beyond the time required for establishing a steady-state flowfield. Temperature distribution obtained for a 1263-K-airflow case is shown in Fig. 7. This is computed using LLNL mechanism and flame was not established as autoignition did not take place. However, when the airflow temperature was increased by another degree to 1264 K autoignition took place and a steady flame similar to that shown in Fig. 1 was established.

Heated air mixes with the relatively cold fuel in the region surrounding the stagnation plane. Simultaneous mixing of fuel and oxygen also takes place. A combination of local equivalence ratio, strain rate and temperature determines whether autoignition can take place or not. Therefore, one should not refer air temperature itself to as autoignition temperature and the ability of a chemical kinetics mechanism in predicting autoignition must be assessed through simulating the entire flowfield. Two-dimensional calculations for autoignition of opposing-jet flow are performed using the three chemical-kinetics mechanisms. It is observed that temperature and OH concentration in the mixing region increase exponen-

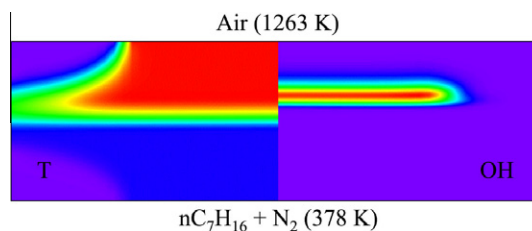


Fig. 7. Flowfield established between opposing jets of heated air and fuel prior to autoignition. Global strain rate is 400 s^{-1} . Temperature distribution between 300 and 1300 K and OH concentration between 0 and 60 ppm are shown in the left and right halves, respectively.

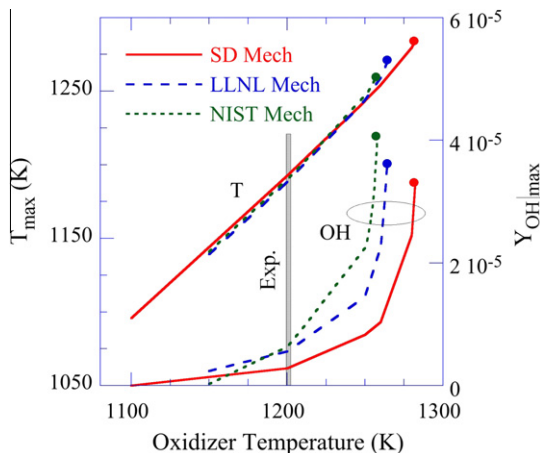


Fig. 8. Maxima in temperature and OH concentration developed between the opposing jets of heated fuel and air jets for different air-jet temperatures. Solid circles represent autoignition conditions.

tially with air temperature. Therefore, for tracing autoignition process, computed results in the form of maximum temperature and OH concentration for different air temperatures are shown in Fig. 8. The conditions at which autoignition took place in the calculations are marked with solid circles. The air temperature at which autoignition took place in the experiment is shown with a hatched rectangle. Among the three mechanisms, NIST mechanism is predicting autoignition process closer to the experiment. On the other hand, one-dimensional calculations performed with LLNL mechanism [31] resulted in autoignition when the air temperature was 1237 K. Current two-dimensional calculation with the same mechanism predicted (Fig. 8) autoignition at 1264 K. In comparison experiment has suggested 1204-K air temperature for autoignition. However, there is about 50-K error margin associated with the measurements made by Seiser et al. [31].

Simulations for the opposing-jet-autoignition experiments are useful in validating a chemical-kinetics model. However, diffusion of fuel, oxygen and radical species in these simulations influence the ignition process and complicate the analyses of ignition chemistries used in the mechanisms. Traditionally, chemical-kinetics mechanisms are evaluated for their ignition characteristics through the investigation of ignition delay times at different temperatures. Calculations for the ignition delay times of a stoichiometric fuel-air mixture at 1-atm pressure are performed using UNICORN code with SD, LLNL, and NIST mechanisms for various temperatures and the results are shown in Fig. 9. These homogeneous ignition calculations are performed in a tube with adiabatic and slip-wall boundary conditions. Results obtained by Seiser et al. [31] for the LLNL mechanism with CHEMKIN code are also shown in Fig. 9 with filled circles. In general, ignition delay times

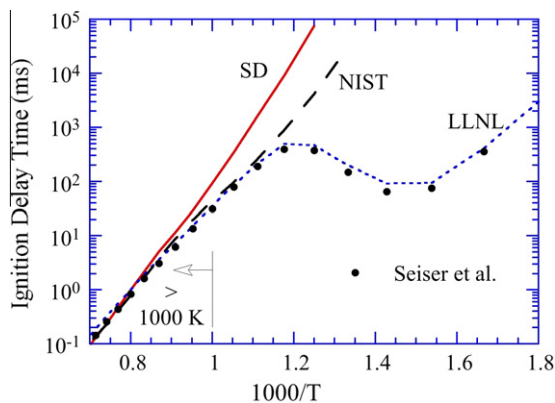


Fig. 9. Ignition delay times of homogeneous stoichiometric mixture of *n*-heptane vapor and air at different temperatures.

increased rapidly when the temperature of the mixture is decreased up to 900 K. LLNL mechanism predicted a drop in ignition delay time before raising further (NTC or negative-temperature-coefficient region) for temperatures less than 900 K. UNICORN code with LLNL mechanism has reproduced the ignition characteristics including the NTC region computed by Seiser et al. [13]. On the other hand, both the SD and NIST mechanisms yielded monotonically increasing ignition delay times. Once again, even though NIST mechanism has the highest number of species, it failed to predict the NTC region of heptane ignition curve. However, ignition delay times exceeding 10 ms are of academic interest only and most of the practical combustion systems require temperatures >1000 K for ignition purpose. All three mechanisms yielded nearly the same ignition delay times for temperatures >1000 K. Interestingly, the homogeneous-mixture calculations (Fig. 9) performed at 1263 K resulted 0.81, 0.89, and 0.62 ms delay times for the SD, LLNL, and NIST mechanisms, respectively, while the opposing-jet-autoignition simulations (Fig. 8) predicted that LLNL mechanism ignites the mixture at lower temperature than the SD mechanism can.

3.4. Partially premixed flame structure

The opposing-jet burner used by Berta et al. [32] for obtaining detailed structures of partially premixed flames consists of upper and lower nozzles and is similar to the burners used in the studies of nonpremixed flames [30,35]. The diameter of each nozzle was 27.38 mm and the separation distance (L) between them was varied between 10 and 20 mm. Fuel in the form of a mixture of pre-vaporized *n*-heptane, air and nitrogen was introduced from the bottom nozzle. Oxidizer was introduced from the top nozzle. A nitrogen curtain was established through an annular duct surrounding the fuel jet in order to isolate the flames from ambient disturbances. Berta et al. [32] also built an annular duct around the top oxidizer nozzle; however, it was used for venting the gases flowed into the burner. While the oxidizer was issued at room temperature, the fuel nozzle was heated and its temperature was controlled for maintaining the fuel-containing stream at 400 K. The fuel vaporizer and mixer are described in Ref. [32].

Four partially premixed flames established in this burner are considered for the evaluation of the chemical-kinetics models. Digital images of these flames are shown in the left half of Fig. 10. The weakly stretched weakly premixed flame in Fig. 10a was obtained with $k = 50 \text{ s}^{-1}$, $\phi = 15.3$, the weakly stretched moderately premixed flame in Fig. 10b was obtained with $k = 50 \text{ s}^{-1}$, $\phi = 2.5$, the moderately stretched moderately premixed flame in Fig. 10c was obtained with $k = 150 \text{ s}^{-1}$, $\phi = 4.1$ and, finally, the moderately

stretched weakly premixed flame in Fig. 10d was obtained with $k = 150 \text{ s}^{-1}$, $\phi = 12.6$. A separation of 10 mm between the fuel and oxidizer nozzles was maintained for all the flames except that in Fig. 10b for which the separation distance used was 20 mm. While the images in Fig. 10a, c and d were taken at the same exposure time, the image in Fig. 10b was taken at double the exposure time for compensating the lower luminosity of the flame. The following visual observations were made [32] from the flame photographs in Fig. 10:

- An orange–red zone present below the blue¹ layer in Fig. 10a.
- Green and blue layers are well separated and flame is curved in Fig. 10b.
- Green and blue layers are barely separated in Fig. 10c.
- Merged green and blue layers in Fig. 10d.
- As the stretch is increased and/or the level of premixing is reduced, the premixed reaction zone (green layer) moves closer to the nonpremixed zone (blue layer), i.e., the separation between the two layers decreases.

Two-dimensional simulations for the *n*-heptane partially premixed flames at different strain rates and equivalence ratios (ϕ) are made using UNICORN code and with SD, LLNL, and NIST chemical-kinetics mechanisms. Boundary conditions, including the suction from the outer duct of oxidizer nozzle, were matched to those used in the experiment. Computational results obtained with LLNL mechanism for the four flames in the left half of Fig. 10 are shown in the right half. Temperature distributions between the upper and lower nozzles are plotted in the left half of the computed flames and soot distributions are shown in the right halves. Note that the flames computed with the other two mechanisms (SD and NIST) also yielded temperature and soot structures identical to those shown in Fig. 10. Shapes of the computed flames matched well with those seen in the experiment. The weakly stretched moderately premixed flame (Fig. 10b) is curved all the way from the center to the edge, while the other three flames are curved only near the edges and yielded flat-flame regions near the center. Simulations made after replacing the suction boundary condition for the oxidizer-side (top) outer duct with an inflow boundary condition similar to that used for the fuel-side (bottom) outer duct yielded nearly flat flames for all the four cases [49], even though gravitational forces were included in the calculations. This suggests that the flame curvatures (especially, near the edges) seen in Fig. 10 are due to the suction employed in the experiment – but not because of the gravitational force acting on the hot products.

A comparison of calculated temperature and soot distributions of all the flames in Fig. 10 suggest that the weakly stretched moderately premixed flame (Fig. 10b) is the thickest and the weakly stretched weakly premixed flame (Fig. 10a) is the sootiest. These predictions matched well with the observations made in experiments. In general, soot surfaces in all these flames are located on the fuel side (bottom) of the peak-temperature surface (red color). However, a careful examination of the computed results reveals that soot surface of the flame in Fig. 10a is significantly away from the peak-temperature surface and this separation decreases gradually as we move through Fig. 10a–b flames. This is consistent with the digital images from experiments. Soot typically forms on the fuel side of a nonpremixed flame [50,51] and on the products side of a premixed flame [52]. The soot-temperature structure of the partially premixed flame in Fig. 10a exhibits predominantly that of a nonpremixed flame and soot surface moves closer to the peak-temperature surface as in Fig. 10b–d as the influence of

¹ For interpretation of color in Fig. 10, the reader is referred to the web version of this article.

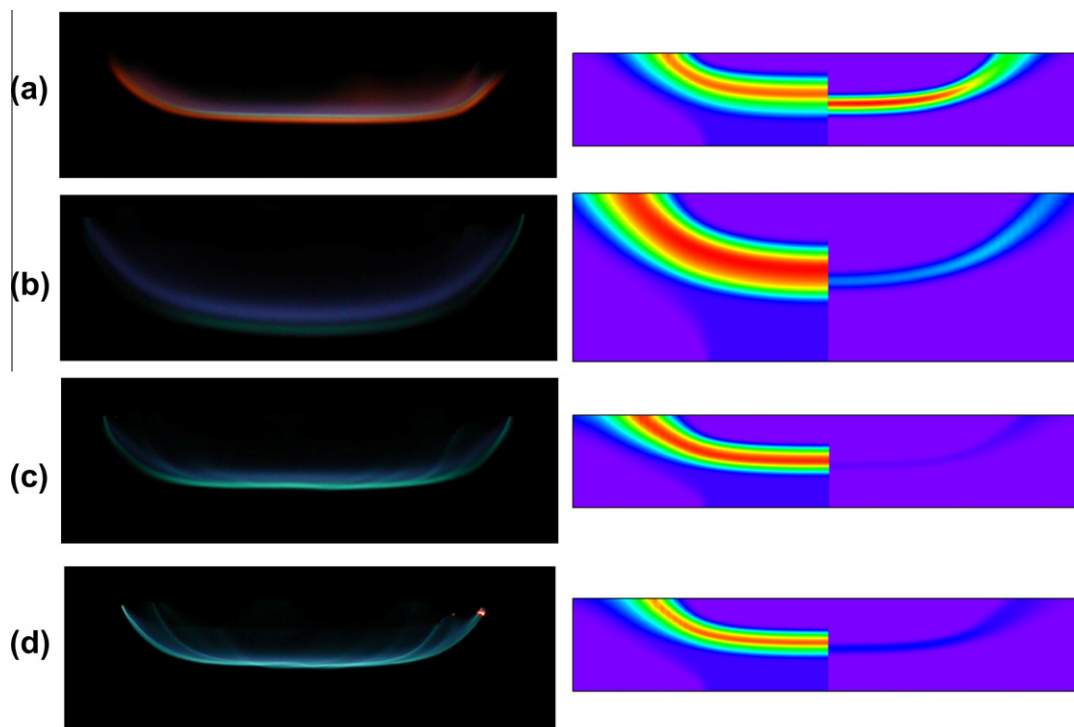


Fig. 10. Actual and simulated opposing-jet partially premixed flames. Direct photographs and simulations made with LLNL mechanism are shown in the left and right halves, respectively for (a) weakly stretched weakly premixed flame, (b) weakly stretched moderately premixed flame, (c) moderately stretched moderately premixed flame, and (d) moderately stretched weakly premixed flame. Distributions of temperature are plotted between 300 and 2100 K in the left halves and distributions of soot between 0 and 1 ppm are shown in the right halves of the computational flames.

premixed combustion increases. Based on the visual chemiluminescence from C_2 species and radiation from CO-oxidation species Berta et al. [32] arrived at the similar conclusions on nonpremixed and premixed reactions in these flames.

Computed structure of the weakly stretched weakly premixed flame (Fig. 10a) along the centerline is compared with measurements in Fig. 11. Flame structures obtained with SD, LLNL, and NIST mechanisms are shown with lines and measurements made with thermocouple and gas chromatograph are shown with symbols. Temperature and reactant species (nC_7H_{16} and O_2) are compared in Fig. 11a, major product species (H_2O , CO_2 , CO , and H_2) are compared in Fig. 11b, fuel fragments (CH_4 and C_2H_2) are compared in Fig. 11c, and, finally, ethylene and butene are compared in Fig. 11d. In general, all three chemical-kinetics mechanisms resulted in nearly the same temperature and reactant and major-product-species concentrations, while significant deviations in the predicted concentrations of fuel fragments are observed. Computed temperature profile matched reasonably with that obtained in the experiment (Fig. 11a), even though the measurements show a broader distribution – especially, on the air side. In fact, when compared with the measurements, the predicted temperatures on the air side are shifted toward the air inlet while the predicted water concentrations on the air side are shifted toward the fuel inlet. This observation is different from that noted in the simulations of experiments conducted by Seiser et al. [30] and cannot be explained with deficiencies in chemical kinetics. Note that the measurements of Berta et al. [32] contained intrusive probes, which could have perturbed the flame and made the distributions shifted. Interestingly, LLNL mechanism predicts the premixed combustion ($z \sim 3$ mm) more distinctly compared to the other two mechanisms and agrees better with the measurements. This is a somewhat surprising result considering the lower autoignition temperature (Fig. 8) obtained with NIST mechanism. The structure of a partially premixed flame is characterized by synergistic

interactions between the two reaction zones, with the nonpremixed zone supported by the intermediate fuels (i.e., CO and H_2) produced in the premixed zone, while the latter is supported by the product species generated in the nonpremixed. These interactions between the premixed and nonpremixed zones make extension of autoignition results to partially premixed flames more difficult or inappropriate. Figs. 11c and d suggest that SD mechanism predicts CH_4 , C_2H_2 and C_2H_4 concentrations better than the other two mechanisms.

Flame structures obtained with the three mechanisms for the weakly stretched moderately premixed flame are shown in Fig. 12. The strong premixed combustion that is causing the temperature to increase at $z \sim 7.5$ mm is well captured by all the three mechanisms. However, LLNL mechanism seems to initiate this premixed combustion slightly upstream where velocity would be higher (in opposing-jet flow velocity decreases with distance from jet exit). Like in the previous case (Fig. 11) measured temperature profile is broader than the predicted ones and is shifted toward oxidizer nozzle (Fig. 12a). Major species concentrations except that of H_2O are well predicted. The one-dimensional calculations performed by Berta et al. [32] using Ranzi's chemical-kinetics model [53,54] also resulted in similar discrepancy in H_2O predictions. Note that since measured H_2O values were obtained through mass balancing of all the other measured species including N_2 , discrepancy between the measurements and calculations for H_2O reflects integrated discrepancy for all the species. Figs. 12c and d indicate a good agreement between the predictions and measurements for different fuel fragments, even though SD mechanism seems to be performing better compared to the other two mechanisms.

Calculations made for the moderately stretched moderately premixed flame are compared with the measurements in Fig. 13. The agreement among the predictions made with different chemical-kinetics models is the best for this flame. Temperature and

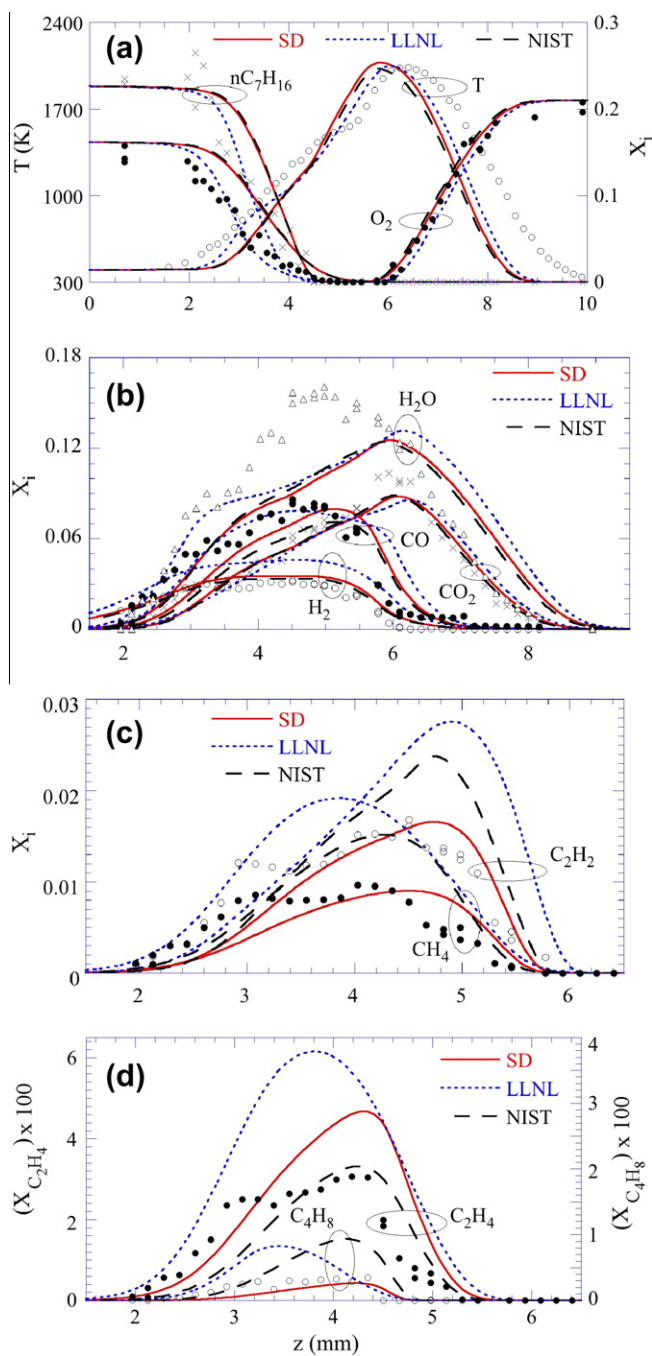


Fig. 11. Comparisons of the structures of the weakly stretched weakly premixed flame simulated using different chemical-kinetics mechanisms (lines) with those measured (symbols). Profiles of (a) temperature and reactant species, (b) major product species, (c) methane and acetylene, and (d) ethylene and butene are compared.

major-product-species-concentration profiles computed with three mechanisms almost lie on top of each other. However, all three mechanisms failed to predict the temperature rise due to premixed combustion seen in the experiment (Fig. 13a). On the other hand, computed nC_7H_{16} , O_2 , H_2 , CO , and CO_2 profiles matched well with the measurements. Contrary to the agreement obtained between the predictions and measurements for CH_4 and C_2H_2 in the previous two flames (Figs. 11c and 12c), these fuel fragments are underpredicted in this moderately stretched moderately premixed flame (Fig. 13c). It is believed that the higher concentrations of CH_4 and C_2H_2 in the experiment led to the development of the premixed-combustion branch.

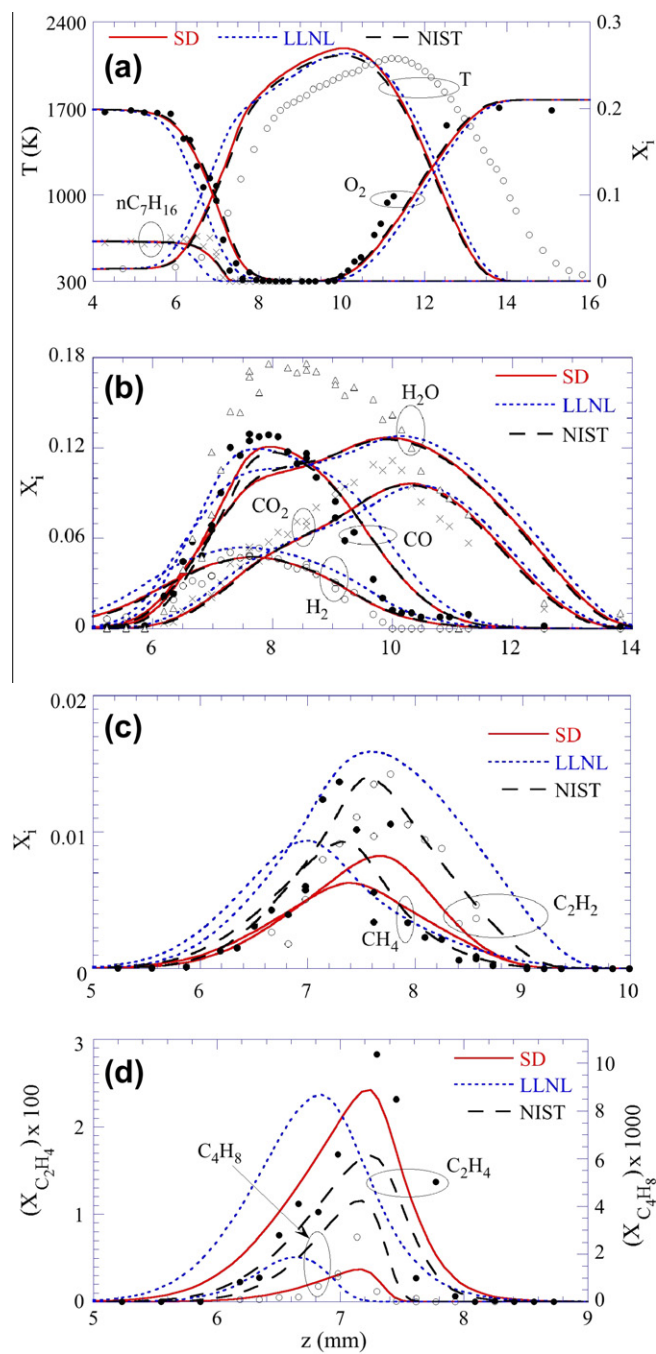


Fig. 12. Comparisons of the structures of the weakly stretched moderately premixed flame simulated using different chemical-kinetics mechanisms (lines) with those measured (symbols). Profiles of (a) temperature and reactant species, (b) major product species, (c) methane and acetylene, and (d) ethylene and butene are compared.

Comparisons between the predictions and measurements for the moderately stretched weakly premixed flame are shown in Fig. 14. Reasonable agreement between the measurements and predictions is obtained for this flame. Once again, the major discrepancies are found in the temperature and water comparisons. Measurements clearly show the premixed-combustion branch in the temperature profile (bulge on the fuel side), while none of the mechanisms predicted such a bulge. Instead, all the mechanisms predicted inflections in the temperature profiles on the fuel side. As shown in Fig. 14d, concentrations of minor fuel fragments are reasonably predicted by the three chemical-kinetics mechanisms.

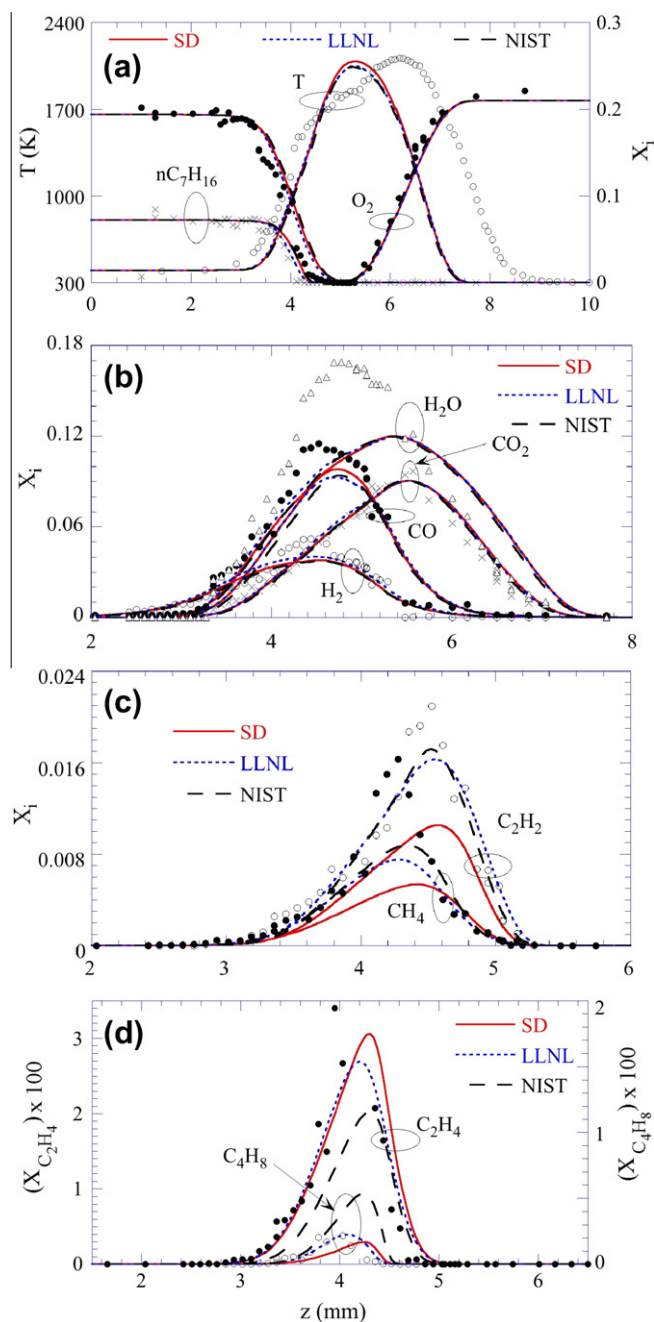


Fig. 13. Comparisons of the structures of the moderately stretched moderately premixed flame simulated using different chemical-kinetics mechanisms (lines) with those measured (symbols). Profiles of (a) temperature and reactant species, (b) major product species, (c) methane and acetylene, and (d) ethylene and butene are compared.

In summary, there are negligible differences between the predictions of the three mechanisms with respect to temperature and major species profiles (nC_7H_{14} , O_2 , CO_2 , CO). However, there are noticeable differences with respect to the intermediate fuel species. For instance, the NIST mechanism predicts less C_2H_4 , but more C_4H_8 compared to the other two mechanisms. The LLNL mechanism predicts more H_2 , while the SD mechanism predicts less C_2H_2 compared to the other mechanisms. LLNL mechanism also consumes nC_7H_{14} and O_2 in the fuel jet faster than the other two mechanisms. All three mechanisms generally reproduced the experimental data in terms of the temperature and major species profiles, although there are some differences with respect to these

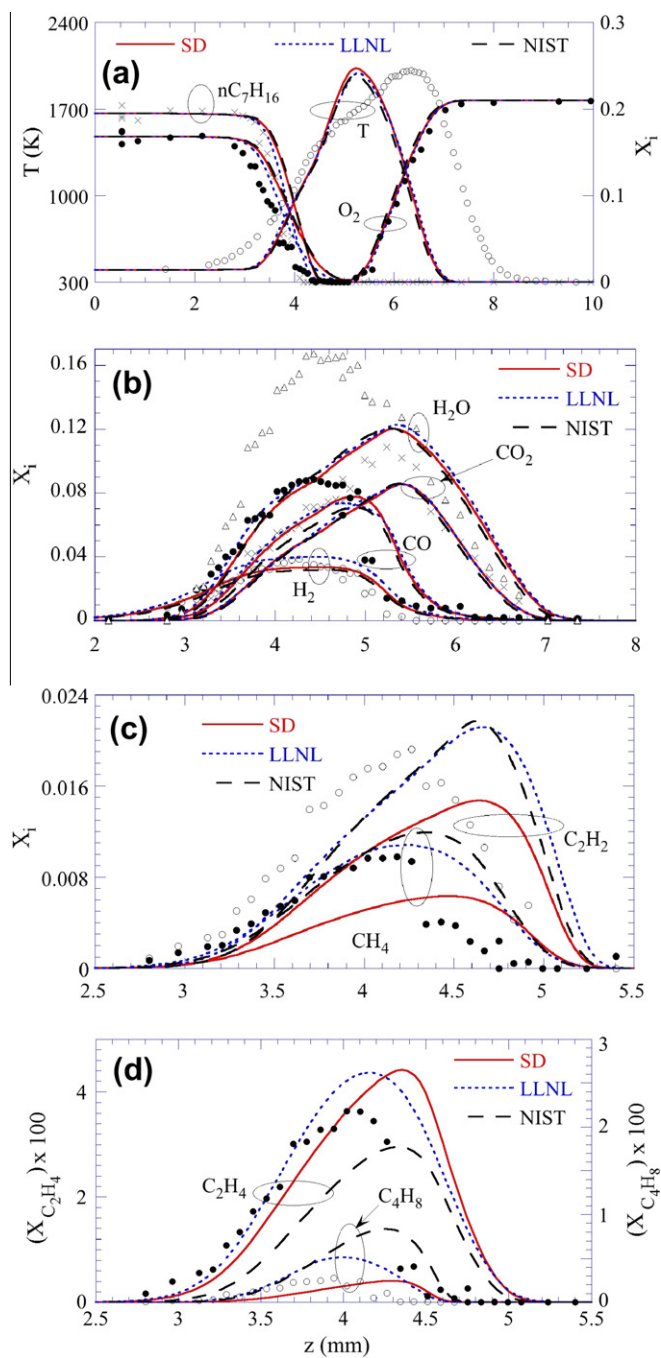


Fig. 14. Comparisons of the structures of the moderately stretched weakly premixed flame simulated using different chemical-kinetics mechanisms (lines) with those measured (symbols). Profiles of (a) temperature and reactant species, (b) major product species, (c) methane and acetylene, and (d) ethylene and butene are compared.

profiles. Predictions locate the peak flame temperature more toward the fuel jet, by about 0.5–1.0 mm, compared to measurements. The peak CO mole fractions are underpredicted by all three mechanisms compared to measurements. The differences between the predictions and measurements are more significant with respect to intermediate species (C_2H_2 , C_2H_4 , C_4H_8), indicating a need for further examination of these mechanisms. The predicted rates of production of these species are slower compared to the measured rates, and their peak mole fractions are generally overpredicted by all three mechanisms compared to measurements. Also, not shown here, benzene (PAH species leading to soot

production) is included only in the NIST mechanism, and its predictions exhibit reasonable agreement with the measured values, although the location of the peak predicted value is shifted slightly toward the oxidizer jet compared to the measurements.

4. Conclusions

A computational study was performed to elucidate the differences in the combustion characteristics predicted by different detailed chemical kinetics modes for *n*-heptane fuel. Three chemical kinetics models, namely (1) San Diego (SD) mechanism (52 species and 544 reactions), (2) Lawrence Livermore National Laboratory (LLNL) mechanism (160 species and 1540 reactions), and (3) National Institute of Standards and Technology (NIST) mechanism (197 species and 2926 reactions) were considered. These mechanisms were incorporated into a time-dependent, two-dimensional, computational-fluid-dynamics model known as UNICORN. Abilities of the numerical models in predicting various diffusion-influenced combustion processes were investigated. Predictions were made for the detailed structures of nonpremixed and partially premixed flames, strain-induced extinction and diffusion-controlled autoignition and the results were compared with the available experimental data. Instead of following the traditional approach of simulating opposing-jet flows with one-dimensional models that utilize assumptions on boundary conditions, two-dimensional simulations for the complete flowfields between the opposing nozzles were made.

Flames formed in the opposing jet burners that used momentum-matched velocities for the fuel and oxidizer are found to be nearly flat even under the influence of gravitational forces. Small curvature toward the oxidizer jet establishes as the diffusion flame forms on the air side of the stagnation plane. The three chemical-kinetics mechanisms considered in this study resulted in nearly the same flame locations, shapes and sizes. Flow and chemical structures along the centerline of a moderately stretched nonpremixed flame are simulated reasonably well. Nearly identical velocity, temperature and major species concentrations are obtained with SD, LLNL, and NIST mechanisms, even though the latter mechanism seems to predict slightly lower peak temperature and CO concentration. Regarding the minor species concentrations none of these three mechanisms gave results consistently comparable to the experiments.

LLNL mechanism predicted the extinction of opposing-jet nonpremixed flame very well. Agreement between the measured and predicted extinction strain rates for a weakly diluted flame was better than that obtained with the same (LLNL) mechanism but with a one-dimensional code. The difference between the extinctions obtained with one- and two-dimensional codes vanished in the diluted-flame case for which extinction strain rate was lower. Flames computed with NIST mechanism extinguished at lower strain rates compared to those computed with the other two mechanisms. On the other hand, NIST mechanism predicted ignition of the opposing-jet flow at lower oxidizer temperatures, which agrees better with the experiment. The inverse temperature dependence or non-monotonic behavior of ignition delay time with respect to increasing temperature in the LLNL mechanism is absent in the other two mechanisms.

The curved opposing-jet partially premixed flames of Berta et al. [32] have been predicted well by the two-dimensional code. Suction from the outer duct surrounding the upper air nozzle used in the experiment for cooling purpose was found to be responsible for curving the flames. Calculations made without such suction yielded nearly flat flames and it was found that the flame structures along the centerline are not affected by this curvature. All three chemical-kinetics mechanisms computed nearly the same

overall shapes for the partially premixed flames although there are some differences in the predicted detailed structures, especially in the premixed-combustion region. LLNL mechanism initiated decomposition of *n*-heptane by about 0.5 mm ahead (toward the fuel duct) of the locations where SD and NIST mechanisms have initiated. However, none of these mechanisms predicted the temperature rise associated with premixed combustion in moderately stretched flames. On a positive note, all three mechanisms correctly predicted the exothermic premixed combustion in a partially premixed flame when stretch rate and premixing were weak.

In general, SD, LLNL, and NIST mechanisms predicted nonpremixed and partially premixed *n*-heptane flames well. Surprisingly, SD mechanism with just one-third of the species used in the other two mechanisms predicted flame structures with nearly the same accuracy. Comparisons with the available experimental data could not suggest which mechanism is better in predicting the minor species concentrations. Computations have underpredicted the concentration of water (not measured directly) in both the nonpremixed and partially premixed flames.

Acknowledgments

This research was conducted on Air Force Contract F33615-03-D-2329 D03, Mr. Charles Frayne Air Force Program Manager. It is jointly funded by the Fuels and Energy Branch of the Energy/Power/Thermal Division of Air Force Research Laboratory (Program Manager Dr. Tim Edwards) and the Strategic Environmental Research and Development Program (SERDP) (Program Manager Mr. Bruce Sartwell). Their support is greatly appreciated.

References

- [1] Wood CP, McDonell VG, Smith RA, Samuelsen GS. Development and application of a surrogate distillate fuel. *J Propul Power* 1989;5(4):399–406.
- [2] Hahandawala MSP, DeWitt MJ, Corporan E, Sidhu SS. Ignition and emission characteristics of surrogate and practical jet fuels. *Energy Fuels* 2008;22:3673–9. doi:10.1021/ef800303a.
- [3] Pitz WJ, Cernansky NP, Dryer FL, Egolfopoulos F, Farrell JT, Friend DG, et al. Development of an experimental database and kinetic models for surrogate gasoline fuels. SAE 2007 Transactions Journal of Passenger Cars - Mechanical Systems, SAE Paper 2007-01-0175; 2007.
- [4] Colket M, Edwards JT, Williams S, Cernansky NP, Miller DL, Egolfopoulos FN, et al. Development of an experimental database and kinetic models for surrogate jet fuels. 45th AIAA Aerospace Sciences Meeting and Exhibit, AIAA-2007-0770, Reno, NV; 2007.
- [5] Smith GP, Golden DM, Frenklach M, Moriarty NW, Eiteneer B, Goldenberg M, et al. 1999. GRI Mech-3.0: <<http://www.me.berkeley.edu/gri-mech/>>.
- [6] Som S, Sivaramakrishnan R, Brezinsky K, Aggarwal SK. Validation of a detailed chemical kinetic modeling for the high pressure combustion of methane–flame and ignition characteristics. 5th US Combustion Meeting, San Diego, CA; March 25–28, 2007.
- [7] Petersen EL, Kalitan DM, Simmons S, Gilles B, Curran HJ, Simmie JM. Methane/propane oxidation at high pressures: experimental and detailed chemical kinetic modeling. In: Proceedings of the combustion institute, vol. 31; 2007. p. 447–54.
- [8] Westbrook CK, Warnatz J, Pitz WJ. A detailed chemical kinetic reaction mechanism for the oxidation of iso-octane and *n*-heptane over an extended temperature range and its application to analysis of engine knock. *Proc Combust Inst* 1988;22:893–901.
- [9] Lindstedt P. Modeling of the chemical complexities of flames. *Proc Combust Inst* 1998;27:269–85.
- [10] Chaos M, Kazakov A, Zhao Z, Dryer FL. *Int J Chem Kinet* 2007;39(7):399–414.
- [11] Rogg B. RUN1DL—The Cambridge Universal Laminar Flamelet Computer Code. In: Peters N, Rogg B. Editors. Reduced kinetic mechanisms for applications in combustion systems, Lecture Notes in Physics m15, Springer-Verlag, Heidelberg, Germany, 1993, pp. 350–351.
- [12] Lutz AE, Kee RJ, Grcar JF, Rupley FM. OPPDIF: A Fortran program for computing opposed flow diffusion flames. SAND96-8243, Sandia National Laboratories, Livermore, CA; 1996.
- [13] Kee RJ, Miller JA, Jefferson TH. CHEMKIN: A general-purpose, problem-independent, transportable, Fortran, chemical kinetic code package. Technical Report SAND80-8003, Sandia National Laboratories, Livermore, CA; 1980.

- [14] Smooke MD, Lin P, Long MB. Computational and experimental study of a laminar axisymmetric methane-air diffusion flame. *Proc Combust Inst* 1991;23:575–82.
- [15] Ibarreta AF, Sung C-J. Flame temperature and location measurements of sooting premixed bunsen flames by rainbow schlieren deflectometry. *Appl Optics* 2005;44(17):3565–75.
- [16] Roquemore WM, Katta VR, Stouffer SD, Belovich V, Pawlik R, Arstingstall M, et al. Soot studies of laminar diffusion flames with recirculation zones. *Proc Combust Inst* 2009;32:729–36.
- [17] Ferri A. Mixing-controlled supersonic combustion. *Annual Rev Fluid Mech* 1973;5:301–38.
- [18] Takahashi F, Katta VR. Chemical kinetic structure of the reaction kernel of methane jet diffusion flames. *Combust Sci Technol* 2000;155(1):243–79.
- [19] Anna AD, Kent JH, Santoro RJ. Investigation of species concentration and soot formation in a co-flowing diffusion flame of ethylene. *Combust Sci Technol* 2007;179:355–69.
- [20] Liu F, Guo H, Smallwood GJ, Gulder OL. Numerical modeling of soot formation and oxidation in laminar coflow non-smoking and smoking ethylene diffusion flame. *Combust Theory Modeling* 2003;7:301–15.
- [21] Oran ES, Weber Jr JW, Stefaniw EI, Lefebvre MH. A numerical study of a two-dimensional H_2 - O_2 -air detonation using a detailed chemical reaction model. *Combust Flame* 1998;113:147–63.
- [22] Mizobuchi Y, Shinjo J, Ogawa S, Takeno T. A numerical study on the formation of diffusion flame islands in a turbulent hydrogen jet lifted flame. *Proc Combust Inst*. 2005;30:611–9.
- [23] Kaplan CR, Kailasanath K. Flow-field effects on soot formation in normal and inverse methane-air diffusion flames. *Combust Flame* 2001;124(1–2):275–94.
- [24] Bennett BAV, Mcenally CS, Pfefferle LD, Smooke M. Computational and experimental study of axisymmetric coflow partially premixed ethylene/air flames. *Combust Flame* 2001;127:2004–22.
- [25] Haworth DC, Cuenot B, Poinso T. Direct numerical simulation and modeling for lean stratified propane-air flames. *Combust Flame* 2002;128:1–21.
- [26] Maroteaux F, Noel L, Ahmed A. Numerical investigations on methods to control the rate of heat release of HCCI combustion using reduced *n*-heptane with multidimensional CFD code. *Combust Theory Modeling*. 2007;11(4):501–25.
- [27] Ebrahimi H, Malo-Molina F. Numerical Investigation of 2-D and 3-D Multitube Pulse Detonation Using H_2 and JP8 Fuel. AIAA-2004-0465, 42nd AIAA Aerospace Sciences Meeting and Exhibit, Reno, NV; January 05–09, 2004.
- [28] Intel Research Report <<http://tecresearch.intel.com/articles/Tera-Scale/1421.html>>.
- [29] Katta VR, Roquemore WM. Calculation of multidimensional flames using large chemical kinetics. *AIAA J* 2008;46(7):1640–50.
- [30] Seiser R, Truett L, Trees D, Seshadri K. Structure and extinction of non-premixed *n*-heptane flames. *Proc Combust Inst* 1998;27:649–57.
- [31] Seiser R, Pitsch H, Seshadri K, Pitz WJ, Curran HJ. Extinction and autoignition of *n*-heptane in counterflow configuration. *Proc Combust Inst* 2000;28:2029–37.
- [32] Berta P, Aggarwal SK, Puri IK. An experimental and numerical investigation of *n*-heptane/air counterflow partially premixed flames and emission of NO_x and PAH species. *Combust Flame* 2006;145:740–64.
- [33] Roquemore WM, Katta VR. Role of flow visualization in the development of UNICORN. *J Visual* 2000;2:257–72.
- [34] Katta VR, Goss LP, Roquemore WM. Numerical investigations of transitional H_2/N_2 jet diffusion flames. *AIAA J* 1994;32(1):84.
- [35] <http://www-mae.ucsd.edu/~combustion/cermec/Heptane-Reactions/>.
- [36] http://www-cmls.llnl.gov/?url=science_and_technology-chemistry-combustion-nc7h16_reduced_mechanism.
- [37] Tsang W. Progress in the development of combustion kinetics databases for liquid Fuels. *Data Sci J* 2004;3:1–9 [mechanism is available at <<http://kinetics.nist.gov/CKMech/ModelsDisplay.jsp?ModelNum=181>>].
- [38] Poling BE, Prausnitz JM, O'Connell JP. The properties of gases and liquids. 5th International Edition, McGraw Hill Companies, Singapore; 2007 [chapters 9 and 10].
- [39] Lindstedt RP. Simplified soot nucleation and surface growth steps for non-premixed flames. In: Bockhorn H, editor. Soot formation in combustion: mechanisms and models. Heidelberg: Springer-Verlag; 1994. p. 417–39.
- [40] Annon. Computational Submodels, International Workshop on Measurement and Computation of Turbulent Nonpremixed Flames; 2001 <<http://www.ca.sandia.gov/TNF/radiation.html>>.
- [41] Kulander JL. *J Quant Spectrosc Radiat Transfer* 1965;5:253–69.
- [42] Gore JP, Jang JH. *ASME J Heat Transfer* 1992;114:234–42.
- [43] Guo H, Liu F, Smallwood GJ. *Combust Theory Modeling* 2004;8:475–89.
- [44] Liu F, Guo H, Smallwood GJ, Gulder OL. *J Quant Spectrosc Radiat Transfer* 2002;73:409–21.
- [45] Leonard BP. A stable and accurate convective modeling procedure based on quadratic upstream interpolation. *Comput Methods Appl Mech Eng* 1979;19:59.
- [46] Katta VR, Goss LP, Roquemore WM. Simulation of vortical structures in jet diffusion flames. *Int J Numer Methods Heat Fluid Flow* 1994;4:413–24.
- [47] Bollig M, Pitsch H, Hewson JC, Seshadri K. Reduced *n*-heptane mechanism for nonpremixed combustion with emphasis on pollutant relevant intermediate species. *Proc Combust Inst* 1996;26:729–37.
- [48] Katta VR, Hu S, Wang P, Pitz RW, Roquemore WM, Gord JR. Investigation of double-state behavior of the counterflow premixed flame system. *Proc Combust Inst* 2007;31:1055–66.
- [49] Aggarwal SK, Katta VR. Evaluation of chemical kinetics models in predicting heptane-air partially premixed flames. In: Paper no. AIAA-2009-5521, 45th AIAA/ASME/SAE/ASEE joint propulsion conference and exhibit, Denver, CO; August 02–05, 2009.
- [50] McNesby KL, Miziolek AW, Nguyen T, Delucia FC, Skagga RR, Litzinger TA. Experimental and computational studies of oxidizer and fuel side addition of ethanol to opposed flow air/ethylene flames. *Combust Flame* 2005;142:413–27.
- [51] Shaddix CR, Smyth KC. Laser-induced incandescence measurements of soot production in steady and flickering methane, propane, and ethylene diffusion flames. *Combust Flame* 1996;107:418–52.
- [52] Olson KL, Harris SJ, Weiner AM. Characterization of polycyclic aromatic hydrocarbons on soot from premixed flat flames. *Combust Sci Technol* 1987;51(1–3):97–102.
- [53] Goldaniga A, Faravelli T, Ranzi E. The kinetic modeling of soot precursors in a butadiene flame. *Combust Flame* 2000;122(3):350–8.
- [54] Ranzi E, Gaffuri P, Faravelli T, Dagaut P. A wide-range modeling study of *n*-heptane oxidation. *Combust Flame* 1995;103(1–2):91–106.